Sparse EEG Source Localization Using LAPPS: Least Absolute *l*-P (0<p<1) Penalized Solution

Joyce Chelangat Bore, Chanlin Yi, Peiyang Li, Fali Li, Dennis Joe Harmah, Yajing Si, Daqing Guo, Dezhong Yao, Feng Wan, and Peng Xu

Abstract*—*Objective: **The electroencephalographic (EEG) inverse problem is ill-posed owing to the electromagnetism Helmholtz theorem and since there are fewer observations than the unknown variables. Apart from the strong background activities (ongoing EEG), evoked EEG is also inevitably contaminated by strong outliers caused by head movements or ocular movements during recordings.** ***Methods:*** **Considering the sparse activations during high cognitive processing, we propose a novel robust EEG source imaging algorithm, least absolute l-P (0<p<1) penalized solution (LAPPS), which employs the l_1-loss for the residual error to alleviate the effect of outliers and another l_p-penalty norm (p = 0.5) to obtain sparse sources while suppressing Gaussian noise in EEG recordings. The resulting optimization problem is solved using a modified alternating direction method of multipliers algorithm.** ***Results:*** **Simulation study was performed to recover sparse signals of randomly selected sources using LAPPS and various methods commonly used for EEG source imaging including weighted minimum norm estimate, l_1-norm, standardized low resolution electromagnetic tomography and focal underdetermined system solver solution. The simulation comparison quantitatively demonstrates that LAPPS obtained the best performances in all the conducted simulations for various dipoles configurations under various signal-to-noise ratio on a realistic head model. Moreover, in the localization of brain neural generators in a real visual oddball experiment, LAPPS obtained sparse activations consistent with previous findings revealed by EEG and functional magnetic resonance imaging.** ***Conclusion:*** **This study demonstrates a potentially useful sparse method for EEG source imaging, creating a platform for investigating the brain neural generators.** ***Significance:*** **This method alleviates the effect of noise and recovers sparse sources while maintaining a low computational complexity due to the cheap matrix-vector multiplication.**

***Index Terms*—EEG inverse problem, ill-posed, outliers, sparse sources, visual oddball.**

I. Introduction

THE scalp electroencephalogram (EEG) represents electrical activity produced by vast numbers of neurons firing within the brain. This can be used to infer the location of the current density sources that generate given EEG potentials, for example epileptic spikes or somatosensory evoked potentials [1], [2]; a similar problem is found in magnetoencephalogram (MEG) [3]. The EEG inverse problem involves calculation of the neural electric current sources locations and magnitudes given a set of electric potentials measured on the scalp surface and the associated positions of those measurements, and the geometry and conductivity properties within the head. This is an underdetermined problem as it lacks a unique solution due to the infinite number of currents distributions inside the head which are compatible with the measured recordings at the head surface [4].

In order to convert data from the EEG recordings on the scalp domain to the sensor domain, an EEG forward model is generated [5]. Solving the EEG forward problem involves a lead field matrix $A \in \mathbb{R}^{m\times n}$ (m indicates the scalp electrodes while n indicates the sources vectors) which signifies the propagation of the electromagnetic field from the sources to the sensors. In the EEG inverse problem, we aim to estimate the actual source locations and orientations inside the brain based on recordings of the electrical potential at the scalp of the head. In other words we seek to recover the source vector $x \in \mathbb{R}^{n\times 1}$ (produced by neuronal generators) from a set of linear measurement $y = Ax$ where $y \in \mathbb{R}^{m\times 1}$ is a measurement vector observed on the $m$scalp electrodes and notably $m < n$ as EEG inverse problem is ill-posed. Considering the noisy nature of the EEG recordings, the linear problem can be mathematically modeled as:

$$y = Ax + \alpha \tag{1}$$

and $\alpha \in \mathbb{R}^{m\times 1}$ is the measurement noise. Generally, $x \in \mathbb{R}^{n\times 1}$ comprises of either dipoles [6]–[8], charges [9]–[11]

Manuscript received July 23, 2018; revised October 10, 2018 and November 9, 2018; accepted November 9, 2018. Date of publication November 14, 2018; date of current version June 21, 2019. This work was supported in part by the National Natural Science Foundation of China under Grants 61522105, 81330032, 61603344, 81401484, and 81771925, in part by the Open Foundation of Henan Key Laboratory of Brain Science and Brain-Computer Interface Technology (HNBBL17001), and in part by the ChengDu's HuiMin projects of science and technology in 2013. *(Corresponding author: Peng Xu.)*

J. C. Bore, C. Yi, P. Li, F. Li, D. J. Harmah, and Y. Si are with the Clinical Hospital of Chengdu Brain Science Institute, MOE Key Lab for Neuroinformation, University of Electronic Science and Technology of China.

D. Guo and D. Yao are with the Clinical Hospital of Chengdu Brain Science Institute, MOE Key Lab for Neuroinformation, School of Life Science and Technology, Center for Information in Medicine, University of Electronic Science and Technology of China.

F. Wan is with the Department of Electrical and Computer Engineering, Faculty of Science and Technology, the University of Macau.

P. Xu is with the Clinical Hospital of Chengdu Brain Science Institute, MOE Key Lab for Neuroinformation, School of Life Science and Technology, Center for Information in Medicine, University of Electronic Science and Technology of China, Chengdu 611731, China (e-mail: xupeng@uestc.edu.cn).

Digital Object Identifier 10.1109/TBME.2018.2881092

or potential [12]. In this work, we employed the dipole model.

EEG inverse problem is typically ill-posed according to the electromagnetism Helmholtz theorem [13] and the inherent characteristics of an underdetermined system. A number of methods utilizing the regularization approach have been proposed such as the L2-norm solution popularly known as Ridge [14] which has led to the rise of other approaches such as Minimum-Norm [15]–[16]. A major drawback of minimum norm (MN) solution is that it favors a superficial source whereby the estimated position of a deep source tends to be shallower than the actual situation thus other methods such as the weighted minimum norm estimate (WMNE) solutions, the standardized low resolution electromagnetic tomography (sLORETA), focal underdetermined system solver (FOCUSS) were developed as an improvement to the previous methods [6], [16]–[19]. Nevertheless, several research efforts are still being made in an effort to improve the spatial resolution of these methods. The mixed norm constraints which employ the penalized approach have also been developed and their advantages have been revealed [20], [21]. Besides from the penalized methods, other methods such as the Recursively applied and projected-Multiple signal classification (RAP-MUSIC) [22], Markov chain Monte Carlo (MCMC) [23], [24], and the approaches based on the Bayesian framework such as Variational Bayes (VB), Spatio-Temporally Regularized Algorithm for M/EEG Patch Source imaging (STRAPS), and Bayesian Electromagnetic Spatio-Temporal Imaging of Extended Sources (BESTIES) have been developed to solve EEG inverse problem [25]–[27]. Motivated by the sparse activations in the brain during high cognitive processing as revealed by various recording techniques such as neural spiking, functional magnetic resonance imaging (fMRI) and positron emission tomography (PET), some other methods have also been developed in efforts to obtain a sparse EEG source localization solution such as the self-coherence enhancement algorithm [28], Lp norm iterative sparse source (LPISS) [29], L1 norm solution (i.e., the least absolute shrinkage selection operator (LASSO)) [30], and Solution Space Sparse Coding Optimization (3SCO) [31]. However, these methods portray some instabilities due to their sensitivities to noise including outliers, source configurations and even the initial source distributions [19], [32]–[34].

In real-world applications, EEGs are usually inevitably contaminated by outliers due to eye blinks or head movements [35]. Theoretically, the popularly utilized L2-norm loss function has a tendency of exaggerating the outlier effect due to the square property of the L2 norm [36]–[38]. However, existing sparse source localization approaches still use the L2-norm loss function and only impose sparse constraints on the objective functions, while still omitting the possible effect of outliers on EEG source estimation. Since the L1-loss function has been proven to be less sensitive to outliers as compared to the quadratic function [39]–[46], in this paper, we propose a novel robust and sparse approach for EEG source imaging known as the Least Absolute l-P ($0<p<1$) Penalized Solution (LAPPS) which simultaneously adopts an L1-loss function to measure the residual error and an Lp-penalty term ($p = 0.5$) to constrain the EEG sources. Our approach here adopts the alternating direction method of multipliers (ADMM) approach to efficiently solve the optimization problem [47]. Compared with other existing methods such as l_1-norm solution, sLORETA, the WMNE solution and FOCUSS, the proposed LAPPS shows its superiority for source estimation in terms of sparsity and robustness when Gaussian noise and outliers are included in the EEG recordings. In this paper, we evaluated the algorithm based on simulated dataset and by localizing the sources of a true P300 EEG dataset.

This paper is structured as follows: the method is introduced is Section II. Section III gives the details for the adopted head model and evaluation indexes. In Section IV, the proposed approach was tested and compared with l_1-norm solution, sLORETA solution, WMNE solution and FOCUSS solution. Finally, we have our discussions and conclusions in Section V and VI respectively.

II. Methods

The use of penalized loss functions defines several types of EEG inverse solutions. In this work, we explore the performance of a subset of the methods mostly used for the EEG source estimation, which include sLORETA solution, WMNE solution, l_1-norm solution and FOCUSS solution. These existing methods are briefly introduced in the following Sections A to D while the novel LAPPS method is introduced in Section E. In practical applications, there are two ways of estimating EEG sources: The first aspect is to assume that the sources (dipoles) have fixed positions and directions, and only the magnitudes are varied within certain periods, this is usually represented by the dipole fitting [22], [26], [27]; another aspect involves estimating sources for each time slice, and this approach can theoretically find the instant sources when both positions and magnitude for the concerned time window are varied, sLORETA, FOCUSS and other minimum norm based methods can be divided into this category [5], [6], [19], [29], [31]. Similar to the latter, in current work, we mainly probe the performance of source estimation for the individual time point.

A. Weighted Minimum Norm Estimate (WMNE) Solution

The WMNE solution for equation (1) is expressed as:

$$x\_WMNE = \arg\min \left\{ \| y - Ax \|_2^2 + \lambda \| Wx \|_2 \right\} \quad (2)$$

where $\lambda \geq 0$ is a regularization parameter and W is a weighting matrix. The solution for this minimization problem is:

$$x\_WMNE = A^T (AA^T + \lambda W)^{-1} y \quad (3)$$

When W is the identity matrix, this solution is referred to as the minimum norm estimate (MNE) but this solution is biased by the fact that superficial dipoles tend to project more strongly on the scalp. As for the weighted MNE (WMNE), this effect is corrected by applying a set of weights to the dipoles so that the influence of dipole depth is reduced [16]. Tikhonov regularization is employed to further constrain the solution to find the source vector which minimizes the residual as well as the energy of the source solution [48]. This additional constraint is represented by the second term in (2); the effect of the two terms is balanced by the regularization parameter lambda.

B. sLORETA Solution

The minimum norm estimate inverse solution is known for its incapability of correct localization of deep point sources [5]. Consequently, sLORETA was developed as a step ahead. The MNE solution for equation (1) is expressed as:

$$x\_MNE = \arg\min \left\{ \| y - Ax \|_2^2 + \lambda \| x \|_2 \right\} \tag{4}$$

where $\lambda \geq 0$ is a regularization parameter. The solution for this minimization problem is:

$$x\_MNE = Ty \tag{5}$$

where $T = A^T [AA^T + \lambda H]^+$, with $H \in R^{m \times m}$ as the identity matrix. In sLORETA, the resolution matrix is used to normalize a coarse minimum norm estimate, thus standardizes the x_MNE solution in equation (5) above by estimation of the variance due to the actual sources and due to noise. As such, the variance of the electrical potential is expressed as:

$$S_y = AS_x A^T + S_y^{Noise} = AA^T + \lambda H \tag{6}$$

while the variance of the source vector is given by:

$$S_{x\_MNE} = TS_y T^T = T(AA^T + \lambda H)T^T = A^T [AA^T + \lambda H]^+ A \tag{7}$$

Eventually, the sLORETA solution [6] corresponds to the estimation of standardized source vector power as,

$$x\_sLORETA = x\_MNE_\iota^T \{[S_{x\_MNE}]_{\iota\iota}\}^{-1} x\_MNE_\iota \tag{8}$$

where $x\_MNE_\iota \in R^{3\times 1}$ is the source vector estimated at the ιth voxel; and $[S_{x\_MNE}]_{\iota\iota} \in R^{3\times 3}$ is the ιth diagonal block of matrix S_{x_MNE}.

C. The l_1-Norm Solution

The l_1-norm solution also known as LASSO (Least Absolute Shrinkage Selection Operator) induces the l_1-norm penalty on the coefficients thus forcing some coefficients to be shrunken to zero, in order to obtain a sparse solution. As a solution to the EEG linear system provided in equation (1), LASSO solves the following optimization problem:

$$x\_l_1 = \arg\min \left\{ \| y - Ax \|_2^2 + \lambda \| x \|_1 \right\} \tag{9}$$

where $\lambda \geq 0$ is a regularization parameter. The above equation (9) is a well-known convex optimization problem, which can reach the globally optimal solution via the 'least angle regression' method [49].

D. FOCUSS Solution

Apart from L1 norm solution, FOCUSS is another approach that can obtain a sparse solution iteratively. To achieve FOCUSS solution (x_FOCUSS), a liner transform ($x = Wq$) is made such that equation (1) is now expressed as:

$$\begin{aligned} &\min \| q \| \\ &\text{s.t.}: \quad AWq = y \end{aligned} \tag{10}$$

where W is a $n \times n$ weighted matrix. Moreover, in its kth iteration, W_k is a diagonal matrix constructed from the prior iteration solution denoted as x_{k-1}. As such, FOCUSS solution [19] can be briefly stated using three iterative steps:

$$\begin{aligned} &Step\,1 : W_k = (\text{diag}\,(x_{k-1})) \\ &Step\,2 : q_k = (AW_k)^+ y \\ &Step\,3 : x_k = W_k q_k. \end{aligned} \tag{11}$$

E. Proposed LAPPS Framework of the EEG Inverse Problem

In essence, both LASSO and FOCUSS impose sparsity constraints onto the sources. However, for EEG inverse problem, though the desired sparse activities can be estimated through the sparsity regularization term, artifacts induced in EEG due to the head movement or eye blinks will inevitably influence the final source estimation. As for the approaches for EEG source estimation mentioned above, the fitting error is still measured by the L2 norm, which exaggerates the effect of outliers. To obtain the sparse EEG sources robustly under artifacts conditions, we propose a Least Absolute l-P (0<p<1) Penalized Solution (LAPPS) which is defined as follows:

$$x\_LAPPS = \min_x \left\{ \frac{1}{\eta} \| Ax - y \|_1 + \| x \|_p^p \right\} \tag{12}$$

where the fitting error is measured in the L1 norm space, the l-P(0<p<1) norm regularization is imposed onto the sources, and $\eta > 0$ is the regularization parameter. Theoretically, the first term measures the error in L1 space thus can alleviate the effect of outliers and the second regularization term can guarantee attainment of the sparse EEG sources. In this work, we solve the formulation above based on a modified alternating direction multiplier method (ADMM) framework [47] with non-convex sparsity inducing penalty function. ADMM holds the advantage that it can split some complex objective functions into simpler sub-problems whose solutions can be easily obtained. Consequently, LAPPS solution can be estimated by the following steps:

Step 1: Rewrite the function in (12) as:

$$\min_{x,B} \frac{1}{\eta} \| B \|_1 + \| x \|_p^p \ \text{subject to}\, Ax - y = B \tag{13}$$

Step 2: Define the associated Lagrangian for the function above

$$\begin{aligned} L(B, x, u) = &\frac{1}{\eta} \| B \|_1 + \| x \|_p^p - \langle u, Ax - y - B \rangle \\ &+ \frac{\lambda}{2} \| Ax - y - B \|_2^2 \end{aligned} \tag{14}$$

where $u \in \mathbb{R}^m$ is the Lagrangian multiplier while $\lambda > 0$ is a penalty parameter.

Step 3: Split the function into three simpler subproblems:
For x-subproblem,

$$x^{k+1} = \arg\min_x \left(\| x \|_p^p + \frac{\lambda}{2} \| Ax - y - B^k - \frac{u^k}{\lambda} \|_2^2 \right) \tag{15}$$

For B-subproblem,

$$B^{k+1} = \arg\min_{B} \left(\frac{1}{\eta} \parallel B \parallel_1 + \frac{\lambda}{2} \parallel Ax^{k+1} - y - B - \frac{u^k}{\lambda} \parallel_2^2 \right) \tag{16}$$

Dual update:

$$u^{k+1} = u^k - \lambda \left(Ax^{k+1} - y - B^{k+1} \right) \tag{17}$$

Therefore, we need to find the solutions for x- subproblem and B - subproblem, respectively. Finally, based on the solutions of these subproblems, we perform a dual update as indicated in equation (17).

Step 4: $x - subproblem$

Solving the x-update actually obtains the least squares solution. If we say, let $c^k = y + B^k + u^k/\lambda$ and $t_1(x^k) = A^T(Ax^k - c^k)$ is the gradient obtained for the quadratic term at point $x^k . x^k - \rho_1 A^T(Ax^k - b^k)$.

$$\frac{1}{2} \parallel Ax^k - c^k \parallel_2^2 \approx \frac{1}{2} \parallel Ax^k - c^k \parallel_2^2 + \langle x - x^k, t_1(x^k) \rangle + \frac{1}{2r_1} \parallel x - x^k \parallel_2^2 \tag{18}$$

$$= \frac{1}{2} \parallel Ax^k - c^k \parallel_2^2 + \frac{1}{2r_1} \parallel x - x^k + r_1 t_1(x^k) \parallel_2^2 - \frac{r_1}{2} \parallel t_1(x^k) \parallel_2^2 \tag{19}$$

where $r_1 > 0$ is a proximal parameter. Consequently, x^{k+1} update is computed from a proximal operator (s^k) [50] with

$$s^k = x^k - r_1 A^T(Ax^k - c^k). \tag{20}$$

Step 5: $B - subproblem$

For the nonconvex problem with $p < 1$, a smoothing method is employed such that problem (1) becomes:

$$\min_x \frac{1}{\eta} \parallel Ax - y \parallel_{1,\varepsilon} + \parallel x \parallel_p^p \tag{21}$$

with the smoothed l_1-norm given by:

$$\parallel B \parallel_{1,\varepsilon} = \sum_i \left(b_i^2 + \varepsilon^2 \right)^{\frac{1}{2}} \tag{22}$$

where $\varepsilon > 0$ is an approximation parameter and we have $\lim_{\varepsilon \to 0} \parallel B \parallel_{1,\varepsilon} = \parallel B \parallel_1$, this means that with a sufficiently small ε, $\parallel B \parallel_{1,\varepsilon}$ approximates the l_1-norm of B. Obviously, $\parallel B \parallel_{1,\varepsilon}$ is strictly convex and its gradient is Lipschitz continuous when $\varepsilon > 0$.

As such, problem (21) is reformulated as

$$\min_{x,B} \left(\frac{1}{\eta} \parallel B \parallel_{1,\varepsilon} + \parallel x \parallel_p^p \right) \text{subject to } Ax - y = B \tag{23}$$

with its Lagrangian given by:

$$L_\varepsilon(B, x, u) = \frac{1}{\eta} \parallel B \parallel_{1,\varepsilon} + \parallel x \parallel_p^p - \langle u, Ax - y - B \rangle + \frac{\lambda}{2} \parallel Ax - y - B \parallel_2^2 \tag{24}$$

B-subproblem is now redefined as:

$$B^{k+1} = \arg\min_{B} \left(\frac{1}{\eta} \parallel B \parallel_{1,\varepsilon} + \frac{\lambda}{2} \parallel Ax^{k+1} - y - B - \frac{u^k}{\lambda} \parallel_2^2 \right) \tag{25}$$

Therefore, $\parallel B \parallel_{1,\varepsilon}$ in (23) is approximated by

$$\parallel B \parallel_{1,\varepsilon} \approx \parallel B^k \parallel_{1,\varepsilon} + \langle B - B^k, t_2(B^k) \rangle + \frac{1}{2r_2} \parallel B - B^k \parallel_2^2 \tag{26}$$

where $t_2(B^k) = \nabla \parallel B^k \parallel_{1,\varepsilon}$ with $t_2(B^k)_i = b_i (b_i^2 + \varepsilon^2)^{-\frac{1}{2}}$, and $r_2 > 0$ is an approximation parameter. Finally, the update for B-subproblem is given by

$$B^{k+1} = \frac{r_2}{\lambda \eta r_2 + 1} \left\{ \frac{1}{r_2} B^k - t_2 \left(B^k \right) + \lambda \eta \left(Ax^{k+1} - y - \frac{u^k}{\lambda} \right) \right\}. \tag{27}$$

Based on the above iterative procedure, we obtain the solution for LAPPS. Following the previous work in [45] which proved that the nonconvex penalization with p = 0.5 attains good performance for sparse analysis, we used 0.5 as p value for the proposed equation (12) in current work.

III. Head Model and Evaluation Indexes

A. Head Model

For this analysis, we employed a 3-shell realistic head model derived from eConnectome software [51], [52] for EEG source localization. A high-resolution cortical surface consisting of 41136 triangles was segmented and reconstructed from the Montreal Neurological Institute (MNI) brain images for visualization. For computational efficiency, the calculated source space was formed by a down-sampled cortical surface with 7850 dipoles. Based on the three-shell conduction model with conductivities of the scalp, skull, and inner cerebral tissues assigned in the ratio of 1:1/20:1 [53], [54], the lead field matrix was calculated using a dipole model by boundary element method (BEM) [55] for a 59 electrode system and its dimension was 59×7850. The current dipoles were evenly positioned over the whole cortical surface with their orientations constrained to be perpendicular to the local cortical surface. The strengths of the dipole sources are estimated using the selected inverse algorithm.

B. Evaluation Indexes

The source localization error, $E_{\text{localization}}$

This describes the distance between the simulated source and the source with the maximum power within the sphere neighbouring the simulated source.

$$E_{localization} = (\parallel p_{true} - \hat{p}_{simu} \parallel) \tag{28}$$

where $\hat{p}_{true}$ and p_{simu} denote the spatial positions of the true and estimated sources, respectively.

The source energy error, E_{energy}

This index measures the ability to recover the source energy, which is defined as,

$$E_{energy} = (\parallel s_{simu} - \hat{s}_{\max} \parallel / \parallel s_{simu} \parallel) \tag{29}$$

where s_{simu} is the strength of simulated source and $\hat{s}_{\max}$ is the strength of estimated source with maximum power within a sphere centered at the original simulated source.

IV. Results

A. Simulation Study

Based on the lead field calculated by BEM for the realistic head model obtained from eConnectome software [51], we obtained the simulated scalp EEG signal by using the EEG forward problem. Considering that the signal-to-noise ratio (SNR), source configurations and the spatial distance between sources influence the performance of inverse methods, in current work, we evaluated the performances under various SNRs and randomly generated source configurations and distances between sources. To simulate the actual EEG recordings, both white Gaussian noise and artifacts are introduced into the simulated EEG signal $y \in \mathbb{R}^{m\times 1}$ in equation (1) under -10 dB, -5 dB, 0 dB, 5 dB and 10 dB SNRs. Different number of sources with random positions, amplitudes and distances between sources across the entire brain are generated. Based on the simulated EEG, the proposed LAPPS and other conventional EEG source estimation approaches (i.e., WMNE, L1, FOCUSS and sLORETA) are used to find the sources, which are then used to calculate the corresponding evaluation indexes including position error and energy error using the simulated sources as the ground truth.

To verify the stability of these methods, for each source configuration under defined SNR, the simulation is repeated to generate 200 simulation data for each number of sources (2, 3, and 4) whereby in every run for each number of sources, the positions, amplitudes and distances between sources are randomly generated and also varied noise with random outlier positions and amplitudes are added, then the mean errors across the 200 runs are finally reported. Moreover, to model the typical EEG scenario whereby in actual EEGs strong ocular artifacts are usually observed close to the eyes, we further assume that any three channels close to eye (located in the frontal areas) will be influenced by the ocular artifacts, thus in the simulation, three outliers will be generated and randomly distributed on the channels in the frontal brain area close to eyes.

We add outliers to the simulated EEG signal, as follows: Set the outlier strength in the range of 1.5 to 5 times the maximum amplitude of the corresponding process, also set the outlier occurrence frequencies to 0.05%, occurrence frequency is defined as the ratio between the number of outliers and the sample points. In our work here, the contaminated channel indexes and the positions where the outliers are located are randomly decided. The signal-to-noise ratio (SNR) is defined as:

$$SNR = 10\log_{10}\left(\frac{\sigma^2(Ax^0)}{\sigma^2(noise)}\right) \tag{30}$$

Here $\sigma^2(Ax^0)$ is the variance of the original signal without noise while $\sigma^2(noise)$ is the variance of the noise (both outliers and Gaussian noise). Obviously, a lower SNR (for example -5 dB) delineates a high ability for sources identification and recovery.

Moreover, in the current work, under a defined SNR, we add outliers and Gaussian noise together to the simulated EEG signal as follows: Firstly, as described above we generated the outliers from the Gaussian distribution N ($\mu + 10\,\sigma^2,\ \sigma^2$), where μ and σ^2 denoted the mean and variance of EEG across all channels at the single time slice. Second, based on the predefined SNR, the Gaussian noise with distribution N $(0, \sigma^2 1)$ will be further added to the signal, where $\sigma^2 1$ is the variance of Gaussian noise that is adjusted according to the predefined SNR (signal to noise ratio). Consequently, the mixture noise (Gaussian and outliers) will be:

$$Noise = \frac{n_1}{\sigma(n_1)}\left[10\wedge\left(\frac{-SNR}{20}\right)\right]\sigma(Ax^0) \tag{31}$$

where n_1 indicates the outliers noise, Ax^0 denotes the true signal without noise while σ stands for standard deviation.

The choice of regularization parameters has a large influence on the final source estimation. We estimated the regularization parameters for LASSO and sLORETA by cross-validation as proposed in the related works [6]; [49], while that of WMNE was evaluated by the L-curve similar to that utilized in the eConnectome software [51]. As for the proposed LAPPS, we follow the work in [42]; [45] and determine the regularization parameter in terms of relative error of recovery, which is in essence the Akaike Information Criterion (AIC) [56].

1) Simulation for Two Sources: In this experiment, we evaluate the performances using simulated sparse EEG signals contaminated by noise of various strengths. We simulated two EEG sources, in which the positions and amplitudes of the two dipole sources are both randomly selected in each of the 200 runs. Then following the simulation procedure, both Gaussian noise and artifacts are added to the simulated EEG recording $y \in \mathbb{R}^{m\times 1}$ from equation (1) with different SNRs. Different approaches are adopted to recover the sources from the noisy EEG recording$y \in \mathbb{R}^{m\times 1}$. For each SNR, the simulation is repeated for 200 times. Based on the 200 runs, the mean position error and energy error are calculated and given in Table I at various SNRs of -10 dB, -5 dB, 0 dB, 5 dB and 10 dB. Table I clearly reveals that the different SNRs of noise actually influence the accurate estimation of sources, where the performance gradually declines with the increase of noise contaminated in EEG recordings. However, among the EEG source solutions mentioned here, LAPPS consistently shows the smallest position and energy errors for all the simulated SNRs. To provide a more intuitive comparison of performances among those EEG inverse solutions, we visually display the strength and spatial distributions of true sources and recovered sources estimated under -5 dB SNR for different approaches in Fig. 1(a) and (b), where the source on the realistic head model (i.e., Fig. 1(b)) is exhibited with the normalized scale within 0$\sim$1 by dividing with the maximum source strength.

TABLE I
ENERGY ERROR AND POSITION ERROR UNDER VARIOUS SNRS FOR 2 SOURCES IN THE PRESENCE OF GAUSSIAN NOISE AND OUTLIERS

Method		-10 dB	-5 dB	0 dB	5 dB	10 dB
FOCUSS	$E_{localization}$	0.80 ± 0.33	0.79 ± 0.33	0.78 ± 0.31	0.77 ± 0.31	0.77 ± 0.27
	Eenergy	6.34 ± 6.16	6.21 ± 6.04	5.69 ± 5.93	5.62 ± 5.89	5.43 ± 5.81
LAPPS	Elocalization	0.30 ± 0.16	0.29 ± 0.15	0.21 ± 0.14	0.18 ± 0.12	0.09 ± 0.10
	Eenergy	1.01 ± 1.09	0.79 ± 0.71	0.74 ± 0.67	0.64 ± 0.58	0.51 ± 0.39
L1	Elocalization	0.78 ± 0.36	0.75 ± 0.34	0.73 ± 0.33	0.71 ± 0.32	0.67 ± 0.30
	Eenergy	3.49 ± 4.11	3.40 ± 4.11	3.11 ± 4.10	2.97 ± 3.98	2.94 ± 3.97
WMNE	Elocalization	0.92 ± 0.17	0.91 ± 0.16	0.90 ± 0.16	0.89 ± 0.13	0.89 ± 0.10
	Eenergy	4.35 ± 4.23	4.04 ± 4.18	3.96 ± 4.08	3.88 ± 4.08	3.60 ± 4.02
sLORETA	Elocalization	0.52 ± 1.25	0.48 ± 1.14	0.43 ± 1.02	0.38 ± 0.92	0.33 ± 0.74
	Eenergy	2.14 ± 3.67	1.52 ± 3.23	1.47 ± 3.17	1.38 ± 3.14	0.88 ± 2.47

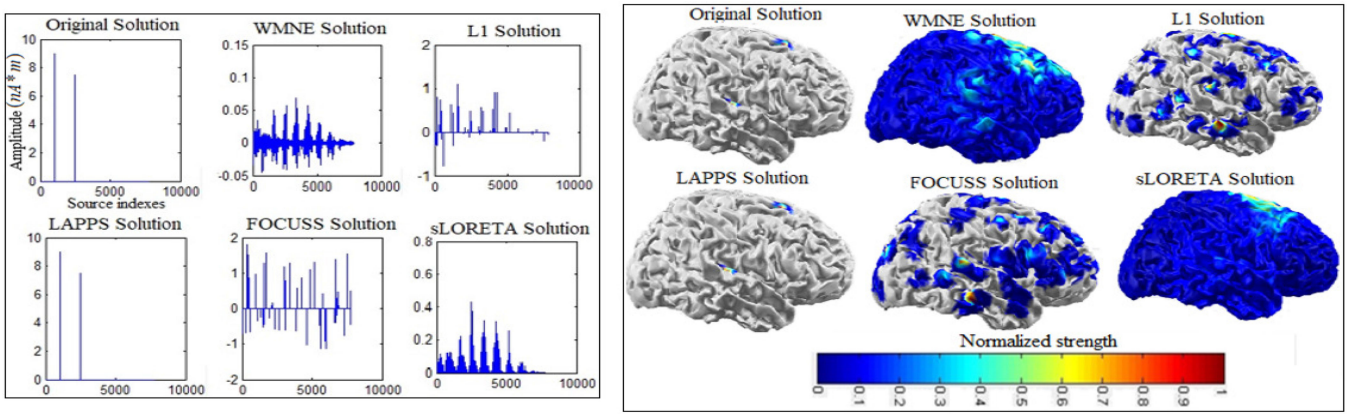

Fig. 1. The inverse solutions for two source configurations under -5 dB SNR. (a) Sources in the indexed solution space. (b) Sources on the realistic head model.

Specifically, Fig. 1(a) shows the solutions for two sources under -5 dB SNR condition for WMNE, L1, LAPPS, FOCUSS and sLORETA in the indexed solution space. Moreover, Fig. 1(b) shows the corresponding source mappings on a realistic head model for the solutions obtained by the five methods.

Apparently, WMNE is too blurred to recover the simulated sources (as expected for L2 norm based methods). sLORETA obtains a better solution with greatly improved resolution than WMNE because sLORETA standardizes the variance of minimum norm estimate to give a better estimation though still blurred. The two sources can be clearly discerned as for FOCUSS and L1 solutions, but they could not obtain the precise strengths of the two sources and also some small spurious sources were generated thus the result was also blurred. LAPPS demonstrates its ability to reconstruct the two simultaneously activated sources as shown in Fig. 1(a) in the indexed solution space and Fig. 1(b) on the realistic head model. This is due to the L1-loss function used which is less sensitive to outliers and the non-convex penalty used to enforce sparsity.

To further reveal the different working mechanisms for those methods, we analyzed the fitted signal after obtaining the inverse solutions, based on which we estimate the recovered simulated EEG signal by forward equation (1). Here we sought to recover the measurement vector $y \in \mathbb{R}^{m \times 1}$ having knowledge of the lead field matrix and the source vector $x \in \mathbb{R}^{n \times 1}$ obtained from each the compared algorithm used in the recovery of two random source vectors. Starting with the original measurement vector (from the 'EEG forward problem') without noise added to it, both Gaussian noise and artifacts are added to the simulated EEG recording $y \in \mathbb{R}^{m \times 1}$ from equation (1) with different SNRs. Various algorithms are used to recover sources (with random positions and energy) from the noisy EEG data then using the estimated source vector and the lead field matrix we recover the fitted signal by each method. We also computed the mean bias in 200 runs for the signals recovered from each method as compared to the original signal without noise. In Fig. 2, the first subfigure shows the original simulated EEG signal and the noised signal while the rest of the subfigures show the original (cyan line) and noised (black line) signals as well as the signals recovered by each method (magenta line) in one of 200 runs. As we can see, LAPPS suppresses the noise and recovers a signal similar to the original simulated EEG signal (the magenta line almost overlaps with the cyan line) and it also obtains the smallest bias as compared to the other algorithms. The other methods have higher bias than LAPPS and actually do fit the signal as well as the outliers because the L2 norm based methods fail to suppress the outliers in the signal.

2) Simulation for Three Sources: Similar to the procedure for the two source configuration, in this section, we present the solutions of WMNE, L1, LAPPS, FOCUSS and sLORETA for three isolated sources under various SNRs. In this simulation,

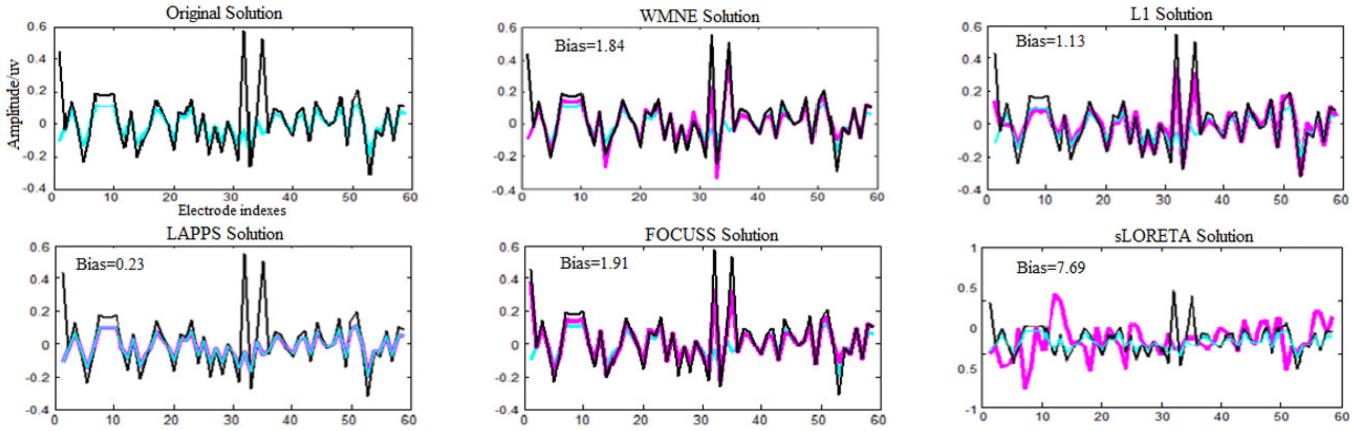

Fig. 2. The recovered EEG signals under −5 dB SNR for the two source configuration in 1 out of 200 runs. The cyan line shows the original signal without noise, the black line shows the noised signal while the magenta line shows the signal predicted by each method. The first subfigure shows the original and the noised signals only while the other subfigures also include the fitted signal predicted by each method.

TABLE II
ENERGY ERROR AND POSITION ERROR UNDER VARIOUS SNRS FOR 3 SOURCES IN THE PRESENCE OF GAUSSIAN NOISE AND OUTLIERS

Method		-10 dB	-5 dB	0 dB	5 dB	10 dB
FOCUSS	$E_{localization}$	0.89 ± 0.34	0.85 ± 0.33	0.85 ± 0.32	0.83 ± 0.31	0.78 ± 0.29
	Eenergy	6.42 ± 6.19	6.32 ± 6.13	6.15 ± 6.07	6.02 ± 6.04	5.57 ± 5.87
LAPPS	Elocalization	0.33 ± 0.17	0.31 ± 0.17	0.26 ± 0.15	0.26 ± 0.13	0.23 ± 0.11
	Eenergy	1.15 ± 1.51	0.83 ± 1.29	0.82 ± 1.09	0.67 ± 1.02	0.60 ± 0.66
L1	Elocalization	0.79 ± 0.36	0.77 ± 0.34	0.77 ± 0.34	0.75 ± 0.33	0.71 ± 0.31
	Eenergy	3.98 ± 4.30	3.81 ± 4.23	3.70 ± 4.22	3.68 ± 4.15	2.95 ± 3.98
WMNE	Elocalization	0.92 ± 0.17	0.91 ± 0.17	0.91 ± 0.16	0.90 ± 0.15	0.89 ± 0.13
	Eenergy	4.49 ± 4.28	4.44 ± 4.18	4.33 ± 4.16	4.31 ± 4.11	3.74 ± 4.07
sLORETA	Elocalization	0.54 ± 1.28	0.51 ± 1.21	0.45 ± 1.04	0.41 ± 1.01	0.36 ± 0.80
	Eenergy	2.15 ± 3.71	2.08 ± 3.49	1.62 ± 3.23	1.40 ± 3.16	1.25 ± 3.04

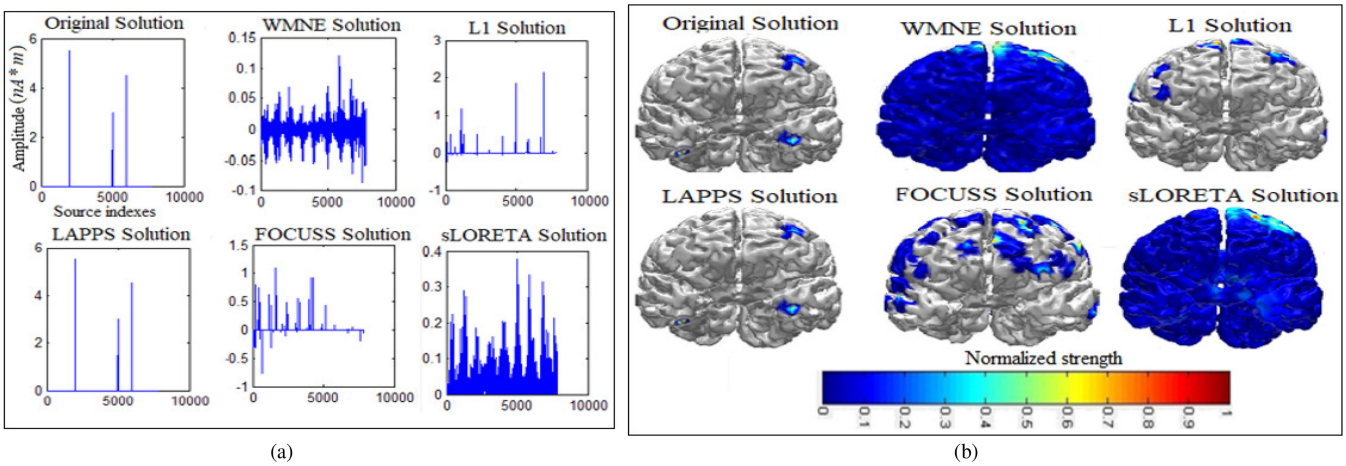

Fig. 3. The inverse solutions for three source configurations under −5 dB SNR. (a) Sources in the indexed solution space. (b) Sources on the realistic head model.

we generated three sparse EEG sources, in which the positions and amplitudes of the three nonzero dipole sources are both randomly selected in each of the 200 runs. The mean position and energy errors under various SNRs are given in Table II for the five approaches, and the specific source information recovered under −5 dB is shown in Fig. 3. Evidently, in Table II and Fig. 3, a similar pattern as that for two sources configuration is observed whereby the source errors become larger with the increasing noise power (i.e., smaller SNR) for all the methods, but LAPPS still obtained the best performance giving the smallest position and energy errors more closer to zero thus yielding the highest spatial resolution. Specifically, we can observe from Fig. 3(b) that WMNE, L1, FOCUSS and sLORETA do not find sparse results for the simulated sources and some spurious

sources are also generated such that the results are quite cloudy. LAPPS produced the best localization here and the three focal sources can be clearly seen.

3) Simulation for Four Sources: Here, we further tested the inverse algorithms in the case of four focal sources localization. We simulated four sparse EEG sources in which the positions and amplitudes of the four nonzero dipole sources are both randomly selected in each of the 200 runs. After these 200 repetitions for each SNR, the mean performances for the five approaches are listed in Table III, where the specific position and energy errors are included. The corresponding source information in the indexed source space and on realistic head model under −5 dB SNR is shown in Fig. 4.

Once again, though the errors are larger compared to those in two and three sources configurations, LAPPS still attained the highest spatial resolution having the least position and energy errors among the five analyzed methods.

B. Simulation for Extended Sources

In the preceding simulations, we focused on a few isolated sources whereby LAPPS proved to be a high resolution algorithm that can accurately reconstruct focal sources. In this section, we will evaluate the performance when sources are extensively distributed not in the isolated pattern. We present the results obtained from the localization of focally extended sources using WMNE, L1, LAPPS, FOCUSS and sLORETA algorithms in in the indexed solution space Fig. 5(a) while in Fig. 5(b) we show the source mappings for all the algorithms here on a realistic head for the extended source configuration.

In this simulation, the neighboring cortex patches enclosed in a 20 mm-radius-sphere with the center at randomly selected positions and having varying strengths across the 200 repeated runs were assumed to be the activated regions. The moment component of each dipole was randomly varied within 0∼10 uv. Background noise including Gaussian noise and outliers are added at −5 dB SNR. For the extended sources, we just simply evaluated if the estimated sources are located in the activated areas because it is difficult to accurately define the position and energy error as isolated sources. The corresponding sources patterns for the true ground and recovered ones in 1 out of 200 runs by the five approaches are given in Fig. 5. By comparing the ground truth (original solution) with the recovered ones, we found that for the noised extended sources, all the methods were unable to precisely recover the sparse sources. Specifically, WMNE estimated a source pattern with activation widely distributed over the cortex; As for L1 norm and FOCUSS, besides from recovering the activation close to the simulated position, other pseudo-activations were also estimated; sLORETA showed its good ability for estimation of the extended sources with most sources located in the due positions; LAPPS achieved a very sparse source pattern, which was located within the sphere enclosing the simulated sources.

C. Real Data Test

We recruited and paid twenty-three postgraduate male subjects (mean age 25.2 years; age range, 24–27 years) who participated in this experiment. All the subjects were healthy with no history of neurological or psychiatric disorder and they all had normal or corrected-to-normal visual acuity. Each participant gave an informed written consent to take part in this study, and the experiment was approved by the review boards of the University of Electronic, Science and Technology of China (UESTC). The classical visual oddball task was utilized and this was implemented through the E-prime 5.0 software.

In this task there were two types of stimuli: the standard (upward-facing triangle consisting of a thin cross in its center, the edge length of the triangle was 4° visual angle) and the target (downward-facing triangle consisting of a thin cross in its center, the edge length of the triangle was 4° visual angle). The two types of stimuli were presented randomly with the target having 0.20 (30 trials) occurrence probability while the standard had 0.80 (120 trials) chance of occurring during each session. The subjects were required to sit approximately 57 cm from the computed monitor. The detailed procedure is illustrated in Fig. 6(a), whereby three task sessions were used. Here, 4 minutes of resting state EEG data was followed by a 1 minute break recording before the visual oddball task performance. In the oddball task, participants were required to fixate their eyes in the center of the screen as much as possible during which the appearance of a bold cross signified the start of the experiment. A thin cross appeared after 250 ms to signify the stimulus onset and this was followed by a standard or target stimulus appearing after 500 ms and its duration was a further 500 ms. The next trial followed after a 1,000 ms break. Participants needed to count the number of target stimuli while ignoring the standard stimuli and reported their counted numbers at the end of the experiment [57], [58].

Electroencephalographic activity was recorded from 64 Ag/AgCl electrodes placed on the scalp according to the 10–20 system. An online filter band of 0.01∼100 Hz (Brain Products GmbH) was employed during the recording and EEG was digitized with a sampling rate of 500 Hz. The reference electrode utilized was FCz while the ground electrode was AFz. Furthermore, two additional channels for vertical and horizontal electrooculograms (EOGs) were placed in the right side of the right eye and below the left eye to monitor the eye movements.

Based on the target and standard stimuli, the recorded EEG was firstly averaged to achieve the two ERPs for each subject. The ERPs were then further averaged across subjects to get the two grand averaged ERPs, i.e., P300 response versus standard response. Fig. 6(c) shows the waveforms for P300 response on all 64 channels, and Fig. 6(b) exhibits the topology of P300 peak approximately at 300 ms after target onset stimulus. Then, based on the topology, we used LAPPS and other EEG inverse approaches to localize the sources accounting for P300 activities. Fig. 6(e) gives the source information estimated by LAPPS, where the generators of the visual P300. Fig. 6(f) shows the corresponding sources estimated by WMNE, L1, FOCUSS and sLORETA, where though the similar source patterns as that of LAPPS could be observed, these methods all result in the blurred and unclear source mappings. These sources estimated by various inverse approaches consistently indicated that distinct attention regions are involved in target stimuli processing,

TABLE III
ENERGY ERROR AND POSITION ERROR UNDER VARIOUS SNRS FOR 4 SOURCES IN THE PRESENCE OF GAUSSIAN NOISE AND OUTLIERS

Method		-10 dB	-5 dB	0 dB	5 dB	10 dB
FOCUSS	Elocalization	0.92 ± 0.38	0.86 ± 0.33	0.85 ± 0.32	0.83 ± 0.31	0.82 ± 0.31
	Eenergy	6.74 ± 6.24	6.36 ± 6.15	6.32 ± 6.07	6.05 ± 6.05	5.91 ± 6.00
LAPPS	Elocalization	0.38 ± 0.18	0.33 ± 0.17	0.29 ± 0.16	0.27 ± 0.13	0.25 ± 0.13
	Eenergy	2.03 ± 2.72	1.66 ± 1.69	1.41 ± 1.24	1.37 ± 1.17	1.11 ± 0.72
L1	Elocalization	0.82 ± 0.41	0.78 ± 0.35	0.78 ± 0.34	0.76 ± 0.34	0.74 ± 0.33
	Eenergy	4.14 ± 4.32	3.82 ± 4.25	3.75 ± 4.25	3.70 ± 4.18	3.36 ± 4.05
WMNE	Elocalization	0.92 ± 0.20	0.91 ± 0.17	0.91 ± 0.17	0.91 ± 0.16	0.90 ± 0.16
	Eenergy	4.91 ± 4.33	4.53 ± 4.22	4.50 ± 4.22	4.37 ± 4.13	4.22 ± 4.11
sLORETA	Elocalization	0.59 ± 1.38	0.53 ± 1.22	0.46 ± 1.05	0.44 ± 1.04	0.38 ± 0.93
	Eenergy	2.51 ± 3.82	2.10 ± 3.60	1.83 ± 3.52	1.72 ± 3.44	1.48 ± 3.21

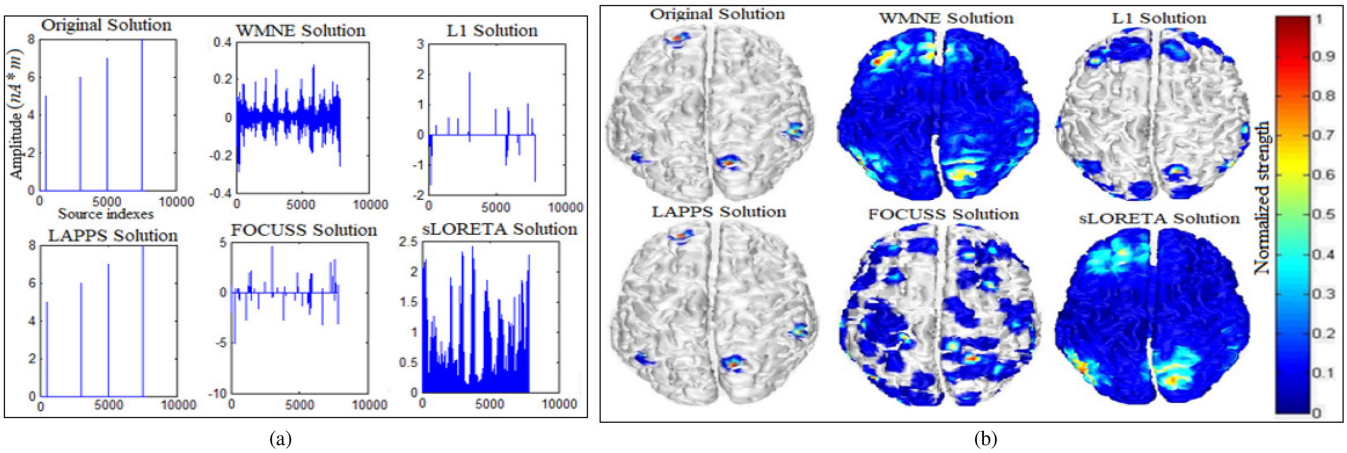

Fig. 4. The inverse solutions for four source configurations under −5 dB SNR. (a) Sources in the indexed solution space. (b) Sources on the realistic head model.

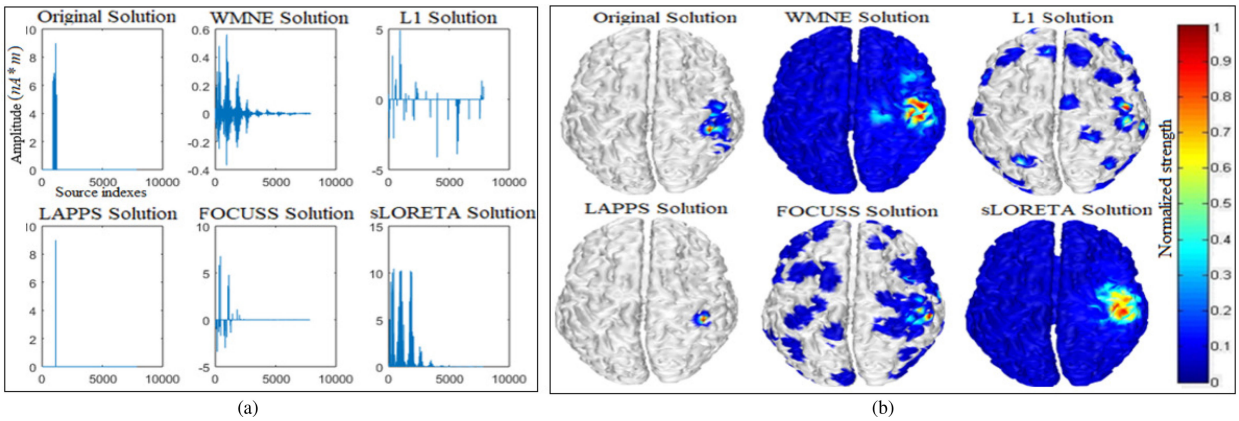

Fig. 5. The inverse solutions for extended sources under −5 dB SNR. (a) Sources in the indexed solution space. (b) Sources on the realistic head mode.

generating the P300 component. To further reveal the activation strength for each paired source areas of the five localized brain areas, we specifically give the detailed source strength for the 10 P300 sources, where the source strength is the maximum strength of the source within the concerned brain areas. Fig. 6(d) shows the strengths of P300 sources in left and right hemispheres in various brain areas including the Superior Temporal Sulcus (STS), Cuneus (Cun), Superior Temporal Lobe (SPL), Precentral Gyrus (PreCG) and the Middle-Frontal Gyrus (MFG) obtained by LAPPS solution.

V. DISCUSSION

Various studies based on fMRI, spikes and intracritinal EEG have proven that brain is sparsely activated during task performance. Therefore, it is reasonable to pursue the sparse solutions for EEG inverse problem. The simulations in the different con-

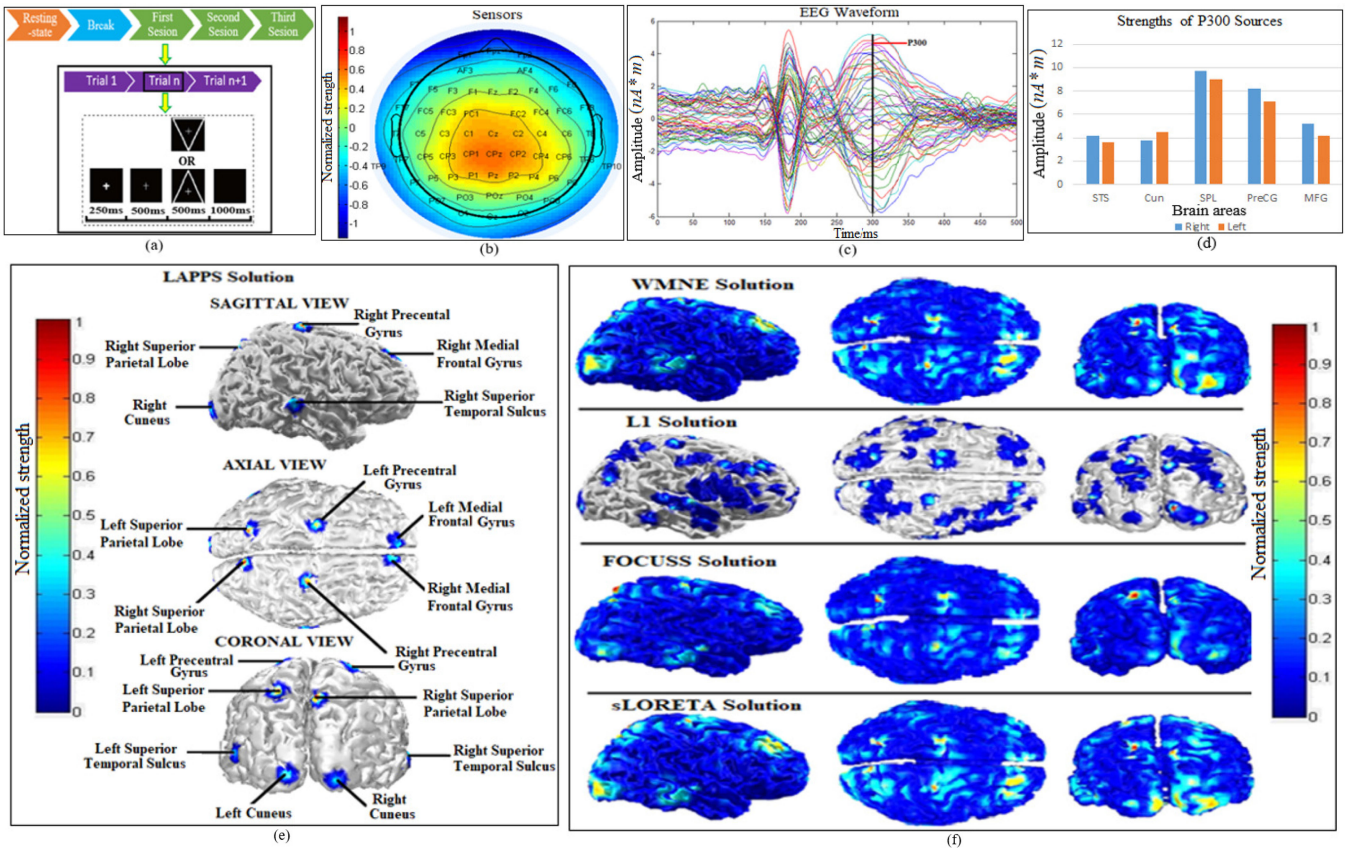

Fig. 6. Source analysis for visual P300 two oddball task. (a) Experimental protocol utilized in this study. (b) Topography distribution of the scalp EEG recording. (c) The EEG waveform obtained from our visual two oddball experiment. (d) Strengths of P300 sources in left and right hemispheres in various brain areas obtained by LAPPS solution. (e) Brain source mappings of the neural generators in the visual P300 two oddball experiment for LAPPS solution. (f) Brain source mappings of the neural generators in the visual P300 two oddball experiment for WMNE solution, L1 solution, FOCUSS solution and sLORETA solution.

ditions including distribution patterns and noise levels actually reveal the different performances among the various EEG inverse solutions. When sources are sparsely distributed, from Fig. 1 and 3∼5, we could observe that LAPPS produced reasonable sparse solutions close to the ground truth, FOCUSS and L1 somewhat depended on the noise level and source configurations, while WMNE and sLORETA generated much blurred results.

By specifically investigating Tables I–III, we could see the influence of source patterns and noise powers on EEG inverse solutions. When signal is corrupted with the increased noise power (i.e., lower SNR), the corresponding performances including position error and energy error for all the approaches decrease, but LAPPS still shows its robustness to noise, still having the smallest bias errors. Besides the noise level, it is also noteworthy that the performance of all the algorithms declines with the increased number of sources from two to three to four active sources being localized as seen in Tables I–III. Though performance is decreased, LAPPS stills performs better in all the simulated source patterns.

The improvement of LAPPS compared with other methods is due to the adaptation of both L1-loss function and Lp-penalty regularization, which can provide the benefits for source estimation from two aspects: one is that L1-loss function is less sensitive to outliers as compared to the quadratic function; another is that the Lp-penalty regularization has been applied in LAPPS to enforce sparsity. Therefore, the WMNE solution and sLORETA which essentially use the minimum norm produce blurred solutions. Though sparse penalty is imposed, FOCUSS and L1 norm still use L2-loss function, obtaining the blurred results in the presence of noise due to their sensitivity to the noise especially the outlier artifacts.

The performance difference among those approaches is due to the different objective functions used to find the solutions, and the unique structure of objective function adopted by LAPPS can guarantee its good performance even under the strong noise background for the isolated sparse sources. In essence, the goal of solving of the EEG inverse problem is to seek the source distribution that can explain the scalp EEG well. When noise especially artifacts usually characterized by large amplitude is introduced to EEG, the widely used L2-loss function manages to fit the outliers that have large contribution to the residuals while neglecting the intrinsic dynamics in EEG. To reveal this difference, after obtaining the source vector estimates from each method (i.e., WMNE, L1, LAPPS, sLORETA and FOCUSS), we further evaluated the performance of these methods by analyzing the predicted signals from their solutions. In other words, after we got the inverse solutions for the source vector

$x \in \mathbb{R}^n$, we then analyzed the fitted scalp EEG series $y \in \mathbb{R}^m$ from equation (1) provided by each methods. Fig. 2 visually shows the different fittings of EEG signals by different inverse approaches when outliers are contained in simulated EEGs.

As shown in Fig. 2, when Gaussian noise with outliers (SNR -5 dB) is added in the two sources simulation, the different inverse approaches actually have different fitting performances. Specifically, WMNE, L1, sLORETA and FOCUSS with the L2-loss function unexpectedly have the outliers fitted to some degree, while the original EEG is not well fitted. Nonetheless, Fig. 2(f) clearly reveals that the predicted signal from LAPPS (magenta line) overlaps with the original signal (cyan line) well, which demonstrates that LAPPS can suppress the outlier artifacts by emphasizing on the fitting of the original EEG, and accounts for the reliable performance under the various levels of SNRs.

In addition, in the simulation test for the focally extended source distribution, strictly speaking, none of concerned inverse approaches could accurately estimate the source patterns. Combining the source patterns in the solution spaces and realistic head model, we could find that these five approaches could estimate a source distribution with the dominating sources closely located within the simulated sphere area. Among the results of WMNE, L1 and sLORETA, LAPPS and FOCUSS, source activations localized by LAPPS were relatively more focal and sparse than all the other methods. This simulation reveals that LAPPS does not reconstruct the whole extent of the entire source maps for extended sources, and LAPPS may converge to an equivalent sparse one thus other methods may be more suitable for the estimation of the extensive sources. The different source patterns obtained by these approaches confirmed that for the EEG inverse problem, different localization methods may result in different equivalent sources, and for different actual problems, the difference among various localization methods should be taken into account [31].

As P300 has been widely used as control signal in brain computer interface [59]–[61], and also serves as an important biomarker to indicate working memory [62], attention [63], etc., its sources have been reliably revealed by using fMRI or EEG [64], [65], which may provide the truth in evaluating the proposed approach when used for the actual EEG dataset. For the real visual EEG data of P300, LAPPS localized the isolated strong sparse activations were observed bilaterally in the superior parietal lobules and pre-central gyrus alongside the minor sparse activations in the medial frontal gyrus, cuneus and superior temporal sulcus as revealed in previous studies on the functional roles of the brain areas [66]–[69].

Consistent with previous studies [70]–[72], our study on the visual two-oddball P300 task particularly revealed predominant activations of the bilateral Superior Parietal Lobules (SPL), a region that has often been observed in paradigms that involve classification of visual stimuli. The SPL involvement in target processing suggests its role in attentional modulation of the contents of working memory through visuo-motor integration. Considering the oddball experiment where there is a high probability of repeated standard stimuli presentations with varied non-target orientations thus the need for categorization and directed attention and this results in higher activity in SPL source.

We also found activations in the middle frontal gyrus (part of the prefrontal cortex) similar to previous studies on visual target stimuli which also revealed a distributed network of neural sources in the middle frontal gyrus (part of the prefrontal cortex) [64], [71]. In addition, previous studies that required subjects to keep a silent count of rare targets without an overt motor response reported the bilateral activation in the premotor and supplementary motor area which may be attributed to planning of an unexecuted motor orienting response or may represent a possible attentional role in sensory processing. We also detected activation of primary visual cortex (cuneus) has been observed in many prior studies involving visual stimulation [72]. Lastly, we also found minor activations in the Superior Temporal Sulcus (STS). It has also been previously found that STS plays a role during visual stimulus processing and participates in target detection [64]. In another study [73] using a visual oddball task, the right STS was shown to have increased connectivity bilaterally with structures involved in memory operations and evaluative processing related to decision making. Besides from the related brain areas accounting for P300 generation, previous study has also reported that P300 amplitude is asymmetric with stronger P300 in the right hemisphere [74]. The quantitative comparison of source strengths between the left and right hemispheres revealed that the four source function areas (superior parietal lobules, pre-central gyrus, medial frontal gyrus and superior temporal sulcus) localized by LAPPS exhibit the stronger activations in the right hemisphere. The domination of the four sources in the right hemisphere may generate the stronger P300 amplitude observed in the right hemisphere [75].

However, as a general EEG component accounting for such high cognition processes like attention, working memory, decision making, the sources of P300 may exhibit the different distribution for the different stimuli. In [64], when the three stimuli oddball task is used, the authors detected other brain areas like Cingulate Gyrus (GC) involved in P300 generation. The three stimuli oddball task enabled them to differentiate the P3b component of the P300 (usually implicated target and distractor detection) from P3a component (mainly evoked by distractor events), whereas our paradigm only evokes P3b. In another study [65] utilizing the same two stimuli oddball task as ours, the source analysis reveals a close source pattern like those revealed by LAPPS.

VI. Conclusion

In this paper we present a new robust EEG source imaging method, the Least Absolute l-P ($p<0<1$) Penalized Solution (LAPPS) by simultaneously using the L1-loss function to measure the residual error and the Lp-sparse constraints to enforce sparse solution. The conducted simulation study proves its superior performance against other existing methods such as the WMNE, FOCUSS, LASSO, and sLORETA when sources are sparsely distributed. The application of LAPPS to an actual P300 dataset also obtained the sparse distribution that is

consistent with previous findings revealed by fMRI and EEG. LAPPS is a potentially useful sparse method for EEG source imaging which we hope will make a significant contribution in the field of cognitive neuroscience and brain imaging and in future enhance the work of clinicians.

References

[1] P. L. Nunez *et al.*, "A theoretical and experimental study of high resolution EEG based on surface Laplacians and cortical imaging," *Electroencephalography Clin. Neurophysiol.*, vol. 90, no. 1, pp. 40–57, 1994.

[2] B. He *et al.*, "Estimating cortical potentials from scalp EEG's in a realistically shaped inhomogeneous head model by means of the boundary element method," *IEEE Trans. Biomed. Eng.*, vol. 46, no. 10, pp. 1264–1268, Oct. 1999.

[3] R. A. Chowdhury *et al.*, "MEG source localization of spatially extended generators of epileptic activity: comparing entropic and hierarchical Bayesian approaches," *PLOS One*, vol. 8, no. 2, 2013, Art. no. e55, 969. doi: 10.1371/journal.pone.0055969.

[4] J. Hadamard, *Lecture on the Cauchy Problem in Linear Partial Differential Equations*, New Haven, CT, USA: Yale Univ. Press, 1923.

[5] R. D. Pascual-Marqui, "Review of methods for solving the EEG inverse problem," *Int. J. Bioelectromagnetism*, vol. 1, no. 1, pp. 75–86, 1999.

[6] R. D. Pascual marqui, "Standardized low-resolution brain electromagnetic tomography (sLORETA): Technical details." *Methods Find. Exp. Clin. Pharmacol.*, vol. 24D, pp. 5–12, 2002.

[7] C. Silva *et al.*, "Evaluation of L1 and L2 minimum norm performances on EEG localizations," *Clin. Neurophysiol.*, vol. 115, no. 7, pp. 1657–1668, 2004.

[8] J. Z. Wang *et al.*, "Magnetic source images determined by a lead-field analysis: the unique minimum-norm least-squares estimation," *IEEE Trans. Biomed. Eng.*, vol. 39, no. 7, pp. 665–675, Jul. 1992.

[9] D. Yao, "The equivalent source technique and cortical imaging. Electroencephalography," *Clin. Neurophysiol.*, vol. 98, no. 6, pp. 478–483, 1996.

[10] D. Yao, "High-resolution EEG mapping: An equivalent charge-layer approach," *Phys. Med. Biol.*, vol. 48, no. 13, pp. 1997–2011, 2003.

[11] D. Yao *et al.*, "Cortical mapping of EEG alpha power using a charge layer model," *Brain Topography*, vol. 17, no. 2, pp. 65–71, 2004.

[12] R. Grave de Peralta Menendez *et al.*, "Imaging the electrical activity of the brain: ELECTRA," *Human Brain Mapping.*, vol. 9, no. 1, pp. 1–12, 2000.

[13] H. V. Helmholtz, "Ueber einige Gesetze der Vertheilung elektrischer Strome in korperlichen Leitern, mit Anwendung auf die thierischelektrischen Versuche," *Ann. Phys. Chem.*, vol. 89, pp. 211–233, 353–357, 1853.

[14] A. E. Hoerl and R. W. Kennard, "Ridge regression: Biased estimation for nonorthogonal problems," *Technometrics*, vol. 12, no. 1, pp. 55–67, 1970.

[15] J. Z. Wang *et al.*, "Magnetic source images determined by a lead-field analysis: The unique minimum-norm least-squares estimation," *IEEE Trans. Biomed. Eng.*, vol. 39, no. 7, pp. 665–675, Jul. 1992.

[16] R. D. Pascual-Marqui *et al.*, "Low resolution electromagnetic tomography: A new method for localizing electrical activity in the brain," *Int. J. Psychophysiol.*, vol. 18, no. 1, pp. 49–65, Oct. 1994.

[17] L. Ding and B. He, "Sparse source imaging in EEG with accurate field modeling," *Human Brain Mapping*, vol. 29, no. 9, pp. 1053–1067, 2008.

[18] J. Yao and P. A. Dewald, "Evaluation of different cortical source localization methods using simulated and experimental EEG data," *NeuroImage*, vol. 25, no. 2, pp. 369–382, 2005.

[19] I. F. Gorodnitsky and B. D. Rao, "Sparse signal reconstruction from limited data using FOCUSS: Are-weighted minimum norm algorithm," *IEEE Trans. Signal Proces.*, vol. 45, no. 3, pp. 600–616, Mar. 1997.

[20] P. A. Valdes-Sosa *et al.*, "EEG source imaging with spatio-temporal tomographic nonnegative independent component analysis," *Human Brain Mapping*, vol. 30, no. 6, pp. 1898–1910, 2009.

[21] M. Vega-Hernandez *et al.*, "Penalized least squares methods for solving the EEG inverse problem," *Statistica Sinica*, vol. 18, pp. 1535–1551, 2008.

[22] J. C. Mosher *et al.*, "Multiple dipole modeling and localization from spatio-temporal MEG data," *IEEE Trans. Biomed. Eng.*, vol. 39, no. 6, pp. 541–547, Jun. 1992.

[23] T. Auranen *et al.*, "Bayesian analysis of the neuromagnetic inverse problem with l-p norm priors," *NeuroImage*, vol. 26, no. 3, pp. 870–884, 2005.

[24] A. Nummenmaa *et al.*, "Hierarchical Bayesian estimates of distributed MEG sources: Theoretical aspects and comparison of variational and MCMC methods," *NeuroImage*, vol. 35, no. 2, pp. 669–685, 2007.

[25] D. Wipf and S. Nagarajan, "A unified Bayesian framework for MEG/EEG source imaging," *NeuroImage*, vol. 44, no. 3, pp. 947–966, 2009.

[26] K. Liu *et al.*, "STRAPS: A fully data-driven spatio-temporally regularized algorithm for M/EEG patch source imaging," *Int. J. Neural Syst.*, vol. 25, no. 4, 2015, Art. no. 1550016.

[27] K. Liu *et al.*, "Bayesian electromagnetic spatio-temporal imaging of extended sources with Markov Random Field and temporal basis expansion," *NeuroImage*, vol. 139, pp. 385–404, 2016.

[28] D. Yao and B. He, "A self-coherence enhancement algorithm and its application to enhancing 3D source estimation from EEGs," *Ann. Biomed. Eng.*, vol. 29, no. 11, pp. 1019–1027, 2001.

[29] P. Xu *et al.*, "Lp norm iterative sparse solution for EEG source localization," *IEEE Trans. Biomed. Eng.*, vol. 54, no. 3, pp. 400–409, Mar. 2007.

[30] R. Tibshirani, "Regression shrinkage and selection via the Lasso," *J. Roy. Statist. Soc. B*, vol. 58, no. 1, pp. 267–288, 1996.

[31] P. Xu *et al.*, "Neuroelectric source imaging using 3SCO: A space coding algorithm based on particle swarm optimization and L0-norm constraint," *NeuroImage*, vol. 51, pp. 183–205, 2010.

[32] C. M. Michel *et al.*, "EEG source imaging," *Clin. Neurophysiol.*, vol. 115, no. 10, pp. 2195–2222, 2004.

[33] C. Silva *et al.*, "Evaluation of L1 and L2 minimum norm performances on EEG localizations," *Clin. Neurophysiol.*, vol. 115, no. 7, pp. 1657–1668, 2004.

[34] Z. Wang *et al.*, "Robust removal of ocular artifacts by combining independent component analysis and system identification," *Biomed. Signal Process. Control*, vol. 10, pp. 250–259, 2014.

[35] B. Blankertz *et al.*, "The non-invasive Berlinbrain–computer interface: Fast acquisition of effective performance in untrained subjects," *NeuroImage*, vol. 37, pp. 539–550, 2007.

[36] H. Wang *et al.*, "L1-norm-based common spatial patterns," *IEEE Trans. Biomed. Eng.*, vol. 59, no. 3, pp. 653–662, Apr. 2012.

[37] P. Li *et al.*, "Autoregressive model in the Lp norm space for EEG analysis," *J. Neurosci. Methods*, vol. 240, pp. 170–178, 2015.

[38] P. Li *et al.*, "Robust granger analysis in Lp norm space for directed EEG network analysis," *IEEE Trans. Neural Syst. Rehabil. Eng.*, vol. 25, no. 11, pp. 1959–1969, Nov. 2017.

[39] J. F. Yang and Y. Zhang, "Alternating direction algorithms for L1-problems in compressive sensing," *SIAM J. Sci. Comput.*, vol. 33, pp. 250–278, 2011.

[40] Y. Xiao *et al.*, "Primal and dual alternating direction algorithms for L1-L1-norm minimization problems in compressive sensing," *Comput. Opt. Appl.*, vol. 54, no. 2, pp. 441–459, 2013.

[41] J. K. Pant *et al.*, "New improved algorithms for compressive sensing based on Lp-Norm," *IEEE Trans. Circuits Syst. II, Express Briefs*, vol. 61, no. 3, pp. 198–202, Mar. 2014.

[42] F. Wen *et al.*, "Robust sparse recovery for compressive sensing in impulsive noise using Lp-norm model fitting," in *Proc. IEEE Int. Conf. Acoust., Speech, Signal Process.*, 2016, pp. 4643–4647.

[43] A. Wagner *et al.*, "Toward a practical face recognition system: Robust alignment and illumination by sparse representation," *IEEE Trans. Pattern Anal. Mach. Intell.*, vol. 34, no. 2, pp. 372–386, Feb. 2012.

[44] S. Foucart and M.-J. Lai, "Sparsest solutions of underdetermined linear systems via Lq-minimization for $0 < q < 1$," *Appl. Comput. Harmon. Anal.*, vol. 26, no. 3, pp. 395–407, May 2009.

[45] F. Wen *et al.*, "Efficient and robust recovery of sparse signal and image using generalized nonconvex regularization," *IEEE Trans. Comput. Imag.*, vol 3, no. 4, pp. 566–579, Dec. 2017.

[46] Y. Wang *et al.*, "Global convergence of ADMM in nonconvex nonsmooth optimization," *J. Scientific Comput.*, pp. 15–62, 2018.

[47] S. Boyd *et al.*, "Distributed optimization and statistical learning via the alternating direction method of multipliers," *Found. Trends Mach. Learn.*, vol. 3, no. 1, pp. 1–122, 2011.

[48] A. N. Tikhonov and V. Y. Arsenin, "Solutions of ill-posed problems," *Amer. Math. Soc.*, vol. 32, no. 144, pp. 1320–1322, 1977.

[49] B. Efron *et al.*, "Least angle regression," *Ann. Statist.*, vol. 32, pp. 407–499, 2004.

[50] Z. Xu *et al.*, "L1/2 regularization: a thresholding representation theory and a fast solver," *IEEE Trans. Neural Netw. Learn. Syst.*, vol. 23, no. 7, pp. 1013–1027, Jul. 2012.

[51] B. He *et al.*, "eConnectome: A MATLAB toolbox for mapping and imaging of brain functional connectivity." *J. Neurosci. Methods*, vol. 195, pp. 261–269, 2011.

[52] F. Babiloni *et al.*, "Estimation of the cortical functional connectivity with the multimodal integration of high-resolution EEG and fMRI data by directed transfer function." *Neuroimage*, vol. 24, no. 1, pp. 118–131, 2005.
[53] Y. Zhang *et al.*, "Estimation of in vivo brain-to-skull conductivity ratio in humans," *Appl. Phys. Lett.*, vol. 89, pp. 223–903, 2006.
[54] T. F. Oostendorp *et al.*, "The conductivity of the human skull: Results of in vivo and in vitro measurements," *IEEE Trans. Biomed. Eng.*, vol. 47, no. 11, pp. 1487–1492, Nov. 2000.
[55] B. He *et al.*, "Electric dipole tracing in the brain by means of the boundary element method and its accuracy," *IEEE Trans. Biomed. Eng.*, vol. BME-34, no. 6, pp. 406–414, Jun. 1987.
[56] J. W. Hardin, *Generalized Estimating Equations (GEE)*, Hoboken, NJ, USA*:* Wiley, 2005.
[57] F. Li *et al.*, "Relationships between the resting-state network and the P3: Evidence from a scalp EEG study," *Scientific Rep.*, vol. 5, 2015, Art. no. 15129, doi: 10.1038/srep15129.
[58] A. Delorme and S. Makeig, "EEGLAB: An open source toolbox for analysis of single-trial EEG dynamics including independent component analysis," *J. Neurosci. Methods*, vol. 134, pp. 9–21, 2004.
[59] Y. Li *et al.*, "An EEG-Based BCI System for 2-D cursor control by combining Mu/Beta rhythm and P300 potential," *IEEE Trans. Biomed. Eng.*, vol. 57, no. 10, pp. 2495–2505, Oct. 2010.
[60] Y. Li *et al.*, "A Hybrid BCI system combining P300 and SSVEP and its application to wheelchair control," *IEEE Trans. Biomed. Eng.*, vol. 60, no. 11, pp. 3156–3166, Nov. 2013.
[61] J. Long *et al.*, "A Hybrid Brain computer interface to control the direction and speed of a simulated or real wheelchair," *IEEE Trans. Biomed. Eng.*, vol. 20, no. 5, pp. 720–729, Sep. 2012.
[62] M. Rangaswamy *et al.*, "A functional MRI study of visual oddball: Evidence for frontoparietal dysfunction in subjects at risk for alcoholism," *NeuroImage*, vol. 21, pp. 329–339, 2004.
[63] J. Polich, "Updating P300: An integrative theory of P3a and P3b," *Clin. Neurophysiol.*, vol. 118, pp. 2128–2148, 2007.
[64] C. Bledowski *et al.*, "Localizing P300 generators in visual target and distractor processing: A combined event-related potential and functional magnetic resonance imaging study," *J. Neurosci.*, vol. 24, no. 42, pp. 9353–9360, Oct. 2004.
[65] A. Dıez *et al.*, "Abnormal frontoparietal synaptic gain mediating the P300 in patients with psychotic disorder and their unaffected relatives," *Human Brain Mapping*, vol. 38, no. 6, pp. 3262–3276, Mar. 2017.
[66] C. Bledowski *et al.*, "Attentional systems in target and distractor processing: A combined ERP and fMRI study," *NeuroImage*, vol. 22, pp. 530–540, 2004.
[67] S. Yantis *et al.*, "Transient neural activity in human parietal cortex during spatial attention shifts," *Nature Neurosci.*, vol. 5, pp. 995–1002, 2002.
[68] J. B. Pochon *et al.*, "The role of dorsolateral prefrontal cortex in the preparation of forthcoming actions: an fMRI study," *Cerebral Cortex*, vol. 11, no. 3, pp. 260–66, 2001.
[69] Y. N. Sokolov *et al.*, *Perception and the Conditioned Reflex*. New York, NY, USA: Macmillian, 1963.
[70] K. A. Moores *et al.*, "Investigating the generators of the scalp Recorded Visuo-Verbal P300 using cortically constrained source localization," *Human Brain Mapping*, vol. 18, pp. 53–77, 2003.
[71] Y. Li *et al.*, "Localizing P300 generators in high-density event-related potential with fMRI," *Med. Sci. Monit.*, vol. 15, no. 3, pp. MT47–53, 2009.
[72] B. A. Ardekani *et al.*, "Functional magnetic resonance imaging of brain activity in the visual oddball task," *Cogn. Brain Res.*, vol. 14, pp. 347–356, 2002.
[73] M. Pail *et al.*, "Connectivity of superior temporal sulcus during target selection," *J. Psychophysiol.*, vol. 30, pp. 29–37, 2016.
[74] J. E. Alexander *et al.*, "P300 hemispheric amplitude asymmetries from a visual oddball task," *Psychophysiology*, vol. 32, pp. 467–475, 1995.
[75] G. Eskikurt *et al.*, "The effect of handedness on visual P300 responses and visual scanning pathways," *Activitas Nervosa Superior*, vol. 55, no. 1/2, pp. 38–50, Mar. 2013.